International Journal of Science and Research (IJSR)
ISSN: 2319-7064
ResearchGate Impact Factor (2018): 0.28 | SJIF (2018): 7.426

Coupled Continuum Advection-Diffusion Model for Simulating Parallel Flow Induced Mass Transport in Porous Membranes

Naveen Daham Weerasekera[1], Aurelie Laguerre[2]

[1, 2] Department of Mechanical and Materials Engineering, Portland State University, Portland, OR-97201, USA

Abstract: ***In this paper, convection-diffusion based mass transport model is proposed for parallel flow driven species transport in microporous membranes. An individual membrane is modeled with the help of macroscopic concentration measurements, considering mass transfer effect in a core of residential energy recovery ventilator sandwiched membrane arrangement, utilizing proton transfer reaction mass spectrometry. Isopropyl alcohol (C_3H_8) is used as the trace compound in experimental analysis. Computational model is developed focusing on a local effect occurring at the sandwiched core structure. Through the model, porous membranes exposed to parallel air flows in both sides are studied. Trace compound injection is modeled by creating constant concentration boundary condition at the channel inlet. Fluid-membrane interface mass transfer is represented by source and sink terms proportional to the interface concentration and transfer coefficients (adsorption and desorption). Mass transport in the membrane is attributed to effective diffusion parameter considering both molecular and Knudsen diffusion processes. In addition, membrane pore size distribution is simplified to a lognormal distribution, with a known mean and standard deviation. The proposed model successfully demonstrated the conjugate transport phenomena in microporous membranes demonstrating the development of concentration boundary layers at the interfaces. Also, it is observed that decrease in adsorption coefficients with the increase of adjacent flow velocities near the membrane. In contrary, increase in desorption coefficient is observed at the interface with the increase of flow velocity. The change in adsorption and desorption parameters in the model confirmed previously reported experimental outcomes.***

Keywords: Membrane Mass Transport, Advection and Diffusion in Mini-Channels, Mass Spectrometry, Numerical Modeling, Monte-Carlo Simulations, Lognormal Pore Size Distribution, Effective Diffusivity

1. Introduction

Membranes are of necessary importance in a variety of applications. Concisely, applications of membranes are distributed among biological to industrial applications [1][2]. Except for application of biological membranes, industry is largely focused on synthetic membranes where these membranes are utilized in a wide range of industrial processes. Some of the common synthetic membrane applications are, separation, ion exchange, microfiltration and ultrafiltration, dialysis, reverse osmosis etc. [3]. In addition to these applications, membranes are widely used in commercial and residential ventilation systems for heat and energy recovery processes [4]. This recovery process is mainly focused on transfer of heat and moisture from air to air [5].

Experimental research on gas transport in membranes are prevalent in literature. Omidkhah et al. [6] studied the facilitated CO_2 transfer in DEA-mediated polyvinyl alcohol (PVA) cross linked with formaldehyde (FA). Their membranes are characterized with Fourier transform infrared spectroscopy (FTIR) and scanning electron microscopy (SEM). In their experiment's highest selectivity for CO_2 (92.72) was recorded from PTFE membranes with PVA/FA 5wt% blend composition. Dahmani et al. [7] studied the membrane fouling in reverse osmosis desalination plant. Mustafa et .al [8] studied the CO_2 separation from various flue gases by using membranes. They reviewed the function of wide variety of membranes on CO_2 separation from polymeric to inorganic construction. Teng et al. [9] reviewed the removal and recovery of organic and inorganic ions from emulsion liquid membranes (ELM). They concluded that ELMs are highly environmentally friendly and they possess a high potential towards greater efficiency. In addition, an important study performed by Pant et al. [10] can be introduced. They performed experimental studies on determining absolute permeabilities and Knudsen diffusivities of PEMFC gas diffusion and microporous layers. They adopted binary friction model (BFM) and Darcy laws to asses these parameters. We also adopted BFM for current study sheltered from their approaches.

When focusing on research performed on membrane transport modeling, firstly, Phattaranawik et al [11] studied the effect of pore size distribution and air flux on mass transport in direct contact membrane distillation. They presented a complete description and effect of pore size in mass transport. They attributed pore size distribution to a lognormal distribution where, it is obtained by using field emission scanning electron microscopy (FESEM). They also recorded mean pore sizes for some of the common membrane types. We utilized their formulation on pore size distribution for our study. Park et al. [12] discussed the attribution of membrane transport to an effective diffusion coefficient. They performed studies on volatile organic compound (VOC) transport in geomembranes in one dimension by using Fick's diffusion laws. In this paper, our work is also based on their hypothesis with only difference in two-dimensional diffusion process. Parallel to our work, Zhang et al. [13] performed study in energy recovery ventilator (ERV) membranes with the help of a computational model. They discussed necessary governing equations of heat and mass transfer in PTFE membranes

used in ERV cores. From their model, they were able to plot the permeability and temperature distribution in a two-dimensional membrane layer as in the application of an ERV.

Among the wide variety of membrane transport models, almost every model is focused on 1-dimensional mass transport process except the work done by Zhang et al. [13]. Computational model of Zhang et al. is limited to quantifying parameter distributions in the membrane surface. As the research gap, coupled mass transfer processes induced by parallel flows are not extensively studied. In this work, we are given an attempt to describe the phenomena by introducing two-dimensional coupled membrane mass transfer model also emphasizing on interfacial mass transfer properties.

As a brief introduction to energy recovery ventilators (ERV), it is a device widely applied in residential and commercial ventilation purpose while saving energy [14]. Focusing on the basis of operation, as in figure 1-(a), ERV removes stale air from indoors and supply fresh air from outdoors back to the indoor space. Under this process, some of the heat and moisture are recovered from indoor stale air, and supplied back to outdoor fresh air. This process is achieved by the component identified as ERV core. ERV core is fabricated by a sandwiched microporous membrane arrangement where, commonly polyethylene or PTFE as membrane materials in industrial practice. Figure 1-(b) shows a typical ERV core. A general ERV consist of four ports as in figure 1, where, two ports are directed towards indoor space and two ports directed to outdoors. These ports are named as in figure 2, and identification of these ports play an important role in this paper.

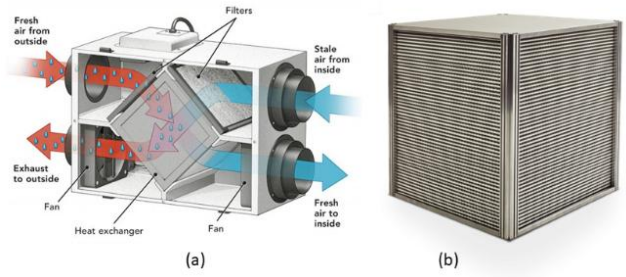

Figure 1: (a). General construction of an ERV and underlying mechanism of transport, (b). Sandwiched porous membrane arrangement of ERV core

In the discussion of ERVs for current application, this device can be used when studying the membrane mass transport performance under induced parallel flows along membrane faces. Huizing et al. [14] intensively studied the mass transfer in ERVs using VOCs. They reported multiple mass transfer efficiencies and permeance values for membranes that are used in ERVs. Their experimental apparatus consists of counter flow induced channel, which is separated by a porous membrane, congruent to ERV process. Also, Nie et al. [15] studied the same mass transfer effect by using a commercial ERV as we used in our study. They were able to document important transfer characteristics of such ERVs from a holistic approach.

Fluid transport properties in the membranes are complex in nature due to the variety of length scales present in the pore structure. Generally, length scales of a membrane can be identified as macroscopic and microscopic [11]. In macroscopic length scale, the order of magnitude between intermolecular collisions and collisions between domain boundaries reaches a higher value. However, in microscopic length scales, this ratio reaches unity making boundary collisions prevalent and it should be considered from an atomic perspective. Macroscopic length scales simply follow the molecular diffusion laws; therefore, flow can be attributed to the help of molecular diffusion coefficient. However, in microscopic length scale, a new diffusion coefficient has to be introduced by considering boundary collisions. A diverse study is performed on this topic by Phattaranawik et al. [11] and Park et al. [12] describing Knudsen diffusion phenomena and application of effective diffusion coefficient in membranes. This theory is broadly discussed in upcoming sections of this paper.

2. Materials and Methods

2.1 Experimental Process Conforming Species Transport in Porous Membranes

Experiments are performed by customarily fabricated experimental rig at the Green Building Research Laboratory of Portland State University. The experimental setup consists of a commercial ERV (Panasonic Intellibalance-1000) with a sandwiched membrane core as in figure 1-(b). Fabricated experimental rig is shown in figure 3.

Experimental process follows by running the ERV subjected to trace compound introduced one of its ports. In the ERV operation, injected trace compound is flowing through channels between membranes in the sandwiched core. Some amount of trace compound is transported by the membranes to opposite direction due to membrane mass transport. We injected the trace compound to the I-Ex (location of the ERV) port as in figure 2, where this port is a suction port. In operation, compound follows I-Ex port to O-Ex port, however, some amount of the compound is returning back from the I-Supp port due to the process mentioned before. By measuring the magnitude of the trace compound concentrations at each port of the ERV, overall transport properties of the ERV core can be assessed.

To measure the concentration of the trace compound proton transfer reaction mass spectrometer (PTR-MS, Ionicon Analytik-800) is used. As the trace compound, we used isopropyl alcohol (C_3H_8O) (volatile organic compound (VOC)) since its high volatility and relatively safe behavior at low ambient concentrations. Concentration measuring ports are marked in green according to figure 2. Isopropyl alcohol is produced and released to the I-Ex ERV port from a Column VOC generator. Maximum concentration of C_3H_8O of the order of $10mg/m^3$ is maintained at the I-Ex port. O-Supp port is supplied with clean laboratory air where concentration of the trace compound (C_3H_8O) is minimum.

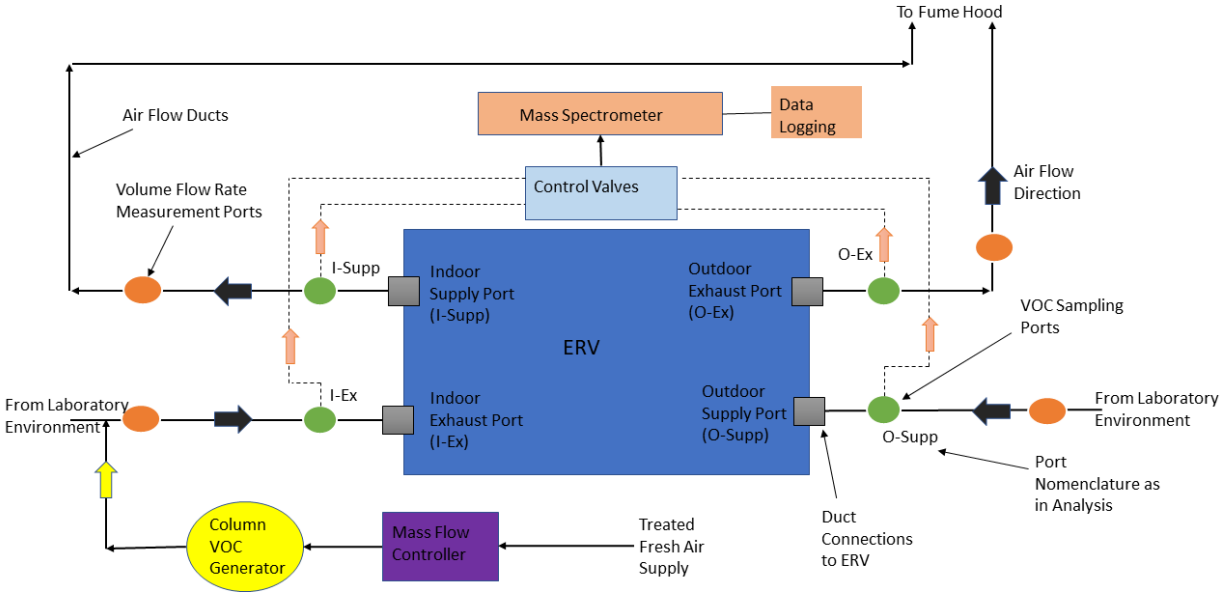

Figure 2: Experimental Apparatus

Both I-Supp and O-Ex ports are directed to outdoors by using the fume hood. This measure is taken to avoid resupply of the trace compound back to the laboratory environment. Live readings of the concentration of trace compound are taken with the mass spectrometer for each ERV port.

2.2. Construction of the Microscale Model

Considering entire ERV sandwiched membrane core as the macroscopic system, we are introducing a microscopic system based on an inlet and exhaust channels separated by a porous membrane in 2D plane. Foundation of this model is depicted in figure 3. As in figure 3-(a) and (b) local phenomena occurring at a complex structure is simplified to its microscopic counterparts. Furthermore, this model is the theoretical representation of the experimental apparatus designed by Huizing et al. [14].

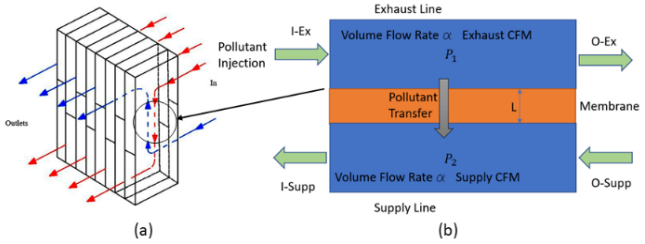

Figure 3: (a). Sectional view of sandwiched core membranes, (b). Underlying transport process in the microscopic model considering individual membrane separated by two mini- fluid channels (Fluid flows are in opposite directions)

Overall volume flow rates of the ERV are proportional to channel flow rate and thus velocity along core channels. At equal average flow velocities in each channel adjacent to membrane, thus, equal pressures are present. Creating, $P_1 = P_2$ in figure 3-(b). This creates an additional advantage on the modeling process, since pressure induced diffusion can be eliminated. Congruent to experimental setup, I-Ex location in the model represents I-Ex ERV port. Therefore, trace compound will be injected on this location. I-Supp location of the model depicts the I-Supp ERV port. Therefore, transported quantity of the trace compound from the membrane is evaluated at I-Supp location.

2.3. Formulation and Numerical Methods

Velocity of a continuum field is described by Navier- Stokes (NS) equations (Eqn. 1), where, u_i is the respective velocity in i^{th} direction on Cartesian coordinates. For laminar flow, turbulent quantities are not present in NS equations. Therefore, NS equations consist with temporal, advection and diffusion terms of the velocity. Velocity source or sink term (**Ч**) can be added accordingly. Where, ν is the kinematic viscosity of the fluid.

$$\frac{\partial u_i}{\partial t} + u_i \frac{\partial u_i}{\partial x_i} = \nu \frac{\partial^2 u_i}{\partial x_i^2} + Ч \qquad (1)$$

For mini channels, very low fluid velocities are present (~0.1m/s). Reynolds numbers, Re<2100 can be given as laminar in nature. Also, unavailability of velocity source or sink term eliminates the Ч term from equation 1. For a channel with rectangular cross section, NS equations simplifies to Poiseuille flow as shown in equation 2. Where in Poiseuille flow, velocity is depending on longitudinal pressure gradient $\frac{\partial p}{\partial x}$ and channel height H. Where, y is the channel height measured from an edge of the channel. Also, Poiseuille flow is derived on the assumption that flow velocity profile remains unchanged on transverse direction. This assumption is applicable for mini channels with large transverse length as in the current case.

$$u = \frac{1}{8\mu}\frac{\partial p}{\partial x}\left(1 - \frac{4y^2}{H^2}\right) \qquad (2)$$

Focusing on fluid flow in pores of membrane, where pore diameters are in the order molecular mean free path, a new parameter called Knudsen number (Kn) is introduced [11]. Knudsen number is simply the ratio between molecular mean free path (λ) and characteristic length (pore diameter- d) **H** of the flow domain. And it is given by,

$$Kn = \lambda/H \quad (3)$$

Where λ can be obtained by cylindrical model for mean free path as,

$$\lambda = \frac{K_B T}{\sqrt{2} p \pi d_g^2} \quad (4)$$

Where, K_B is the Boltzmann constant, T is the absolute temperature, p is the pressure and d_g is the diameter of the cylinder. In addition, diffusion that occurs in higher Knudsen numbers are known as Knudsen diffusion. Mass transport equation for concentration (C) based parametric form can be given as,

$$\frac{\partial c}{\partial t} + u\frac{\partial c}{\partial x} + v\frac{\partial c}{\partial y} = D\frac{\partial^2 C}{\partial x^2} + D\frac{\partial^2 C}{\partial y^2} + \Phi \quad (5)$$

Where, D is the molecular diffusion coefficient and Φ is the mass source or sink term. Where, u , v are velocities in x and y directions in cartesian system. For a flow in mini-channel, since velocity in the y direction is neglected (eqn. 2), advection term containing v is dropped. Also, concentration distributions of the species are uniform along y-direction and it is only a function of x, concentration gradients along y-direction are also dropped. Therefore, final mass transport equation after modifications can be given as,

$$\frac{\partial c}{\partial t} + u\frac{\partial c}{\partial x} = D\frac{\partial^2 C}{\partial x^2} + \Phi \quad (6)$$

Considering mass transport in the membrane, due to very low fluid velocities in micropores, transport properties can be attributed to concentration gradient driven pure diffusion. However, the diffusion parameter must be accompanied by both molecular and Knudsen diffusion processes. Therefore, a new diffusion coefficient called effective diffusion coefficient (D_{eff}) is introduced [12]. Therefore, the mass transport equation at the membrane can be given as in equation 7. Importantly, diffusion process in both x and y directions are considered by respective concentration gradients.

$$\frac{\partial c}{\partial t} = D_{eff}\frac{\partial^2 C}{\partial x^2} + D_{eff}\frac{\partial^2 C}{\partial y^2} \quad (7)$$

Effective diffusion coefficient can be obtained by analogous electrical circuit concept introduced by Phattaranawik et al. [11] as in equation 8. Where, D_{KA} is the Knudsen diffusion coefficient. It is important to note that effective diffusion coefficient D_{eff} is considered as isotropic in the entire membrane. This assumption sufficiently represents the overall membrane diffusion process.

$$\frac{1}{D_{eff}} = \frac{1}{D} + \frac{1}{D_{KA}} \quad (8)$$

Knudsen diffusion coefficient can be obtained from cylindrical model for mean free path for a dilute gas as defined by the binary friction model presented by Pant et. al. [10],

$$D_{KA} = 0.89 \times \frac{1}{3} \times d \times \sqrt{\frac{8RT}{\pi M}} \quad (9)$$

Where, R is the universal gas constant and M is the molecular weight.

Modeling source or sink term Φ performed according to the method introduced by Corsi et al. [16] for porous materials. In this approach, dependence of Φ is attributed to membrane adsorption coefficient (S_a), bulk species concentration at the cells adjacent to the membrane fluid interface (c_{bulk}) and associated interface surface area A.

$$\Phi = S_a . c_{bulk} . A \quad (10)$$

In similar fashion, desorption from the membrane to any adjacent fluid can be given by using membrane desorption coefficient (S_d), membrane fluid interface concentration ($c_{membrane}$) (Measured from membrane surface) and associated surface area.

$$\Phi = -S_d . c_{membrane} . A \quad (11)$$

Finally, Knudsen diffusion coefficient depends on pore diameter (d) as in equation 9. However, the pore size distribution in a membrane is highly randomly distributed. As a solution for this challenge, Monte-Carlo simulations are performed by considering lognormal distribution of pore sizes. This approach is already utilized by Phattaranawik et al. [10], considering lognormal pore size distribution. The average pore size and standard deviation is recorded by manufacturer of the membrane material. Figure 5 represents, computed Knudsen diffusion and effective diffusion coefficients for average pore diameter of 0.2µm. Furthermore, simplified probability density function for lognormal distribution can be given as,

$$d(x) = \frac{1}{x\sigma\sqrt{2\pi}} exp\left(-\frac{(lnx-\mu)^2}{2\sigma^2}\right) \quad (12)$$

Where, d(x) is the diameter of the pore, μ is the mean pore diameter and σ is the standard deviation. Parameter $x = 1$ simplifies the entire distribution to general Gibrat's distribution. Monte Carlo simulations are performed as introduced by He at al.[17].

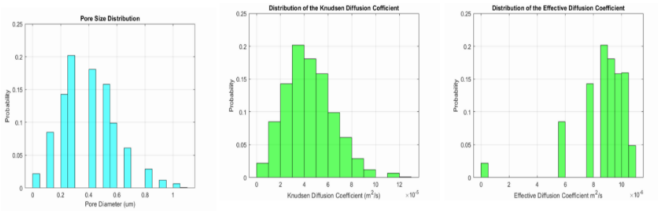

(a) Pore size distribution (b) Distribution of the Knudsen diffusion coefficient (c) Distribution of the effective diffusion coefficient

Figure 4: Monte-Carlo Simulation Results for (a). Cylindrical pore size distribution, (b). Distribution of Knudsen diffusion coefficient, (c). Distribution of the effective diffusion coefficient

From simulation results, most probable effective diffusion coefficient is obtained as 9.2×10^{-6} m^2/s. Since effective diffusion coefficient is in the order of molecular diffusion coefficient, we can infer that Knudsen diffusion has a minor impact on overall diffusion process in these length scales.

In the total model, equations 6 and 7 are solved using finite difference method (FDM) adopting explicit scheme [18]. The boundary conditions pertaining to adsorption and desorption are applied as per equations 8 and 9. A custom

FDM code is constructed and executed in MATLAB software.

Discretized advection diffusion mass transport equation (eqn. 6) according to explicit central differencing scheme can be given as,

$$\frac{C_{i,j}^{n+1}-C_{i,j}^{n}}{\Delta t} = u_i \frac{C_{i+1,j}^{n}-C_{i-1,j}^{n}}{\Delta x} + D\left(\frac{C_{i+1,j}^{n}-2C_{i,j}^{n}+C_{i-1,j}^{n}}{\Delta x^2}\right)+\emptyset \quad (13)$$

Equation 6 is discretized in x-direction with time step Δt and grid spacing of Δx. Where, subscript i depicts the grid points in x-direction and j for y direction. Equation 7 can be discretized by the same scheme as follows,

$$\frac{C_{i,j}^{n+1}-C_{i,j}^{n}}{\Delta t} = D_{eff}\left(\frac{C_{i+1,j}^{n}-2C_{i,j}^{n}+C_{i-1,j}^{n}}{\Delta x^2}\right) + D_{eff}\left(\frac{C_{i,j+1}^{n}-2C_{i,j}^{n}+C_{i,j-1}^{n}}{\Delta x^2}\right)+\emptyset \quad (14)$$

Pollutant injection is demonstrated as, setting a constant concentration boundary condition at the channel entry. Order of magnitude of concentration is determined by the experimental application.

3. Results

3.1 Experimental Outcomes

Figure 6 represents typical concentration measurement taken at each ERV port. ERV port designation is identified as in figures 3 and 5. According to figure 6, values of concentrations at each ERV port can be given as distinctive concentration spikes. Highest spike is obtained at the I-Ex ERV port and lowest at O-Supp port. Parallelly, second highest is observed at O-Ex port and second lowest is obtained at I-Supp port. From this result, it is evident that mass transport process is occurring across the ERV core membranes. I-Ex port has the highest concentration since the trace compound is introduced at I-Ex port as in figure 3. O-Supp port has the lowest concentration since this port is directed towards the ambient where, minimum concentration of the trace compound is present.

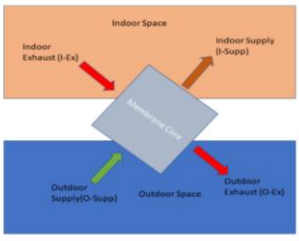

Figure 5: Identification of ports on the ERV as per figure 3

In figure 6, at equal channel flow rates, differences in concentration between I-Ex port and O-Ex port and I-Supp and O-Supp matches in a considerable magnitude. These differences are unable to reach equal values since the leakages of trace compound from the ERV casing.

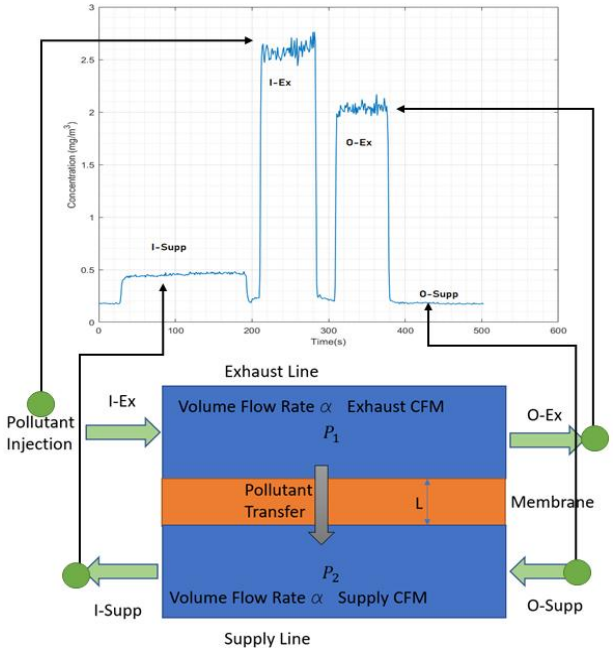

Figure 6: Concentration measurements in designated locations obtained from live mass spectrometry readings

At equal channel flow velocities, advection induced pressure gradient can be eliminated. Therefore, transport in the membrane can be attributed directly to the concentration gradient of the trace compound.

3.2 Simulation Outcomes

In the model, inlet channel, membrane and exit channel are represented by three contour plots as in figure 7-8. Trace compound is injected in the left face of the inlet channel as shown in the same figure. This entry represents I-Ex ERV port in experiments. In addition, figure 7 presents a snapshot in concentration distribution obtained with 0.02s of simulation time. In this time period it is observable that trace compound is not travelled entirely to the opposite end of the channel. However, diffusion is already started in the membrane and concentration boundary layer is developing in the exhaust side.

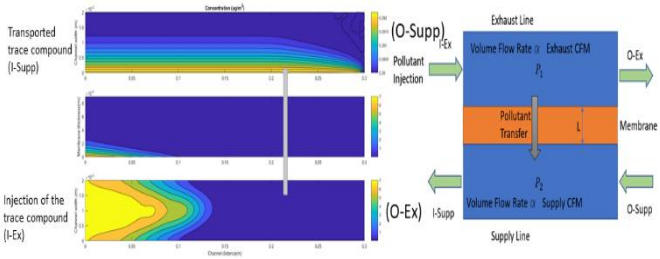

Figure 7: Concentration distribution before attaining steady state

Figure 8 presents a snapshot in concentration distribution after system attained to steady state. Steady state for current model is obtained at 0.06s where, constant concentration at the I-Supp location is observed. Figure 9 represents typical concentration time graphs that utilized for steady state analysis process with fixed S_a and S_d model coefficients.

Figure 10 represents variation of S_a and S_d model coefficients with increasing channel flow rates.

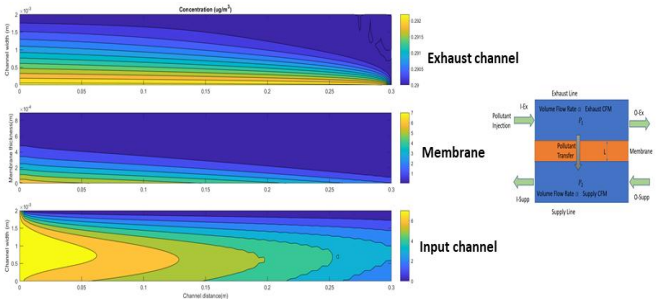

Figure 8: Concentration distribution after attaining steady state

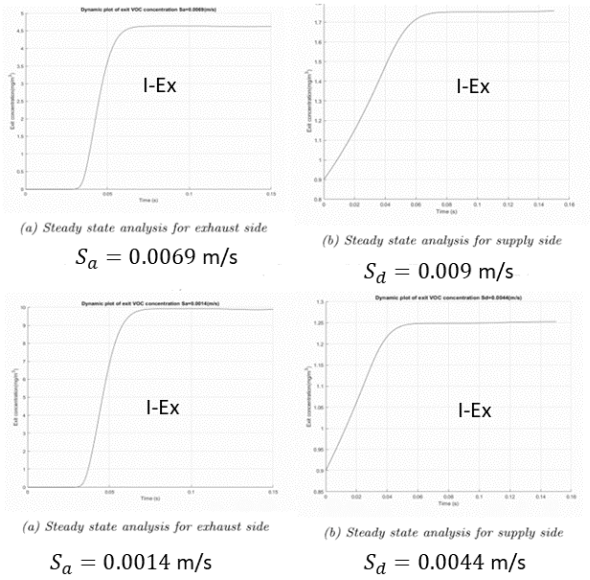

(a) Steady state analysis for exhaust side $S_a = 0.0069$ m/s

(b) Steady state analysis for supply side $S_d = 0.009$ m/s

(a) Steady state analysis for exhaust side $S_a = 0.0014$ m/s

(b) Steady state analysis for supply side $S_d = 0.0044$ m/s

Figure 9: Steady state calibration of the model analyzing variation of concentration at each depicted location in figure 8.

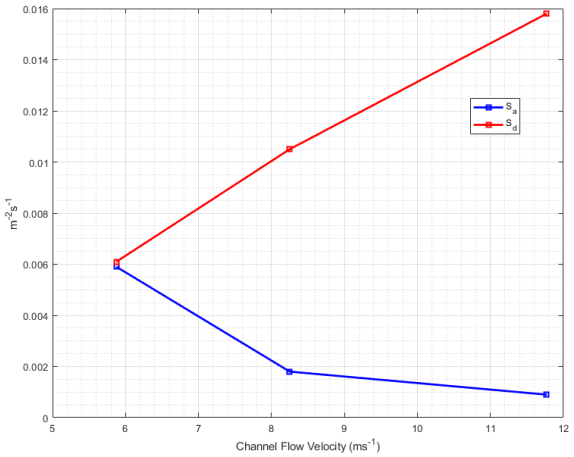

Figure 10: Variation of S_a and S_d coefficients with air flow rate

4. Discussion

From the simulation results, it is observed that concentration of the trace compound in the membrane near to the channel entry is higher than the remaining area. This result clarifies the concentration gradient driven diffusion since concentration at the channel entry is the highest. Initially, concentration boundary layer develops in the channel in the bottom as in figure 8. Then transport follows multidirectional (x and y directions) diffusion pattern in the membrane. Finally, trace compound is exhausting to the top channel creating a desorption concentration boundary layer. Calibrating the model with experimental outcomes, an estimation of effective diffusion coefficient, adsorption and desorption parameters can be obtained. For the current case, we observed S_a and S_d coefficients falls in the order of 10^{-3} where congruent to the magnitude recorded by Corsi et. al. [16]. Increasing the value of these coefficients helps the model to attain steady state faster. Also, when studying the variation of S_a and S_d coefficients with channel flow rates as in figure 10, value of S_a decreases with the increase of channel velocity but at the same time S_d decreases. This result is observed since these coefficients are depending on the individual concentration of trace compound at the fluid-solid interface. And concentration itself depends on the fluid flow velocity. Therefore, at higher advection currents induced by higher velocities, causing trace compound to get transported away from the interface reducing the interface contact time thus reducing the value of S_a. However, opposite effect occurs for the value of S_d coefficient, since increase of advective currents at the transported side providing more flow to the membrane-fluid interface increasing mass transfer from membrane to fluid.

5. Conclusion

In this paper, novel computational model is introduced to mass transport in porous membranes located between two parallel fluid flow streams. The model is enabling to quantify adsorption and desorption parameters of the membrane-fluid interface. However, model must be applied parallel with experimental results to compare membrane properties. Mass transport in the membrane is attributed to an effective diffusion process utilizing an effective diffusion coefficient. Also, pressure induced diffusion is eliminated in this model considering equal flow velocities and equal fluid pressures at each side of the membrane. Decrease of membrane adsorption coefficient is observed with the increase of channel flow velocities. However, increase of desorption coefficient is demonstrated with the increase of channel flow velocities. This result predicts the role of advection near membrane-fluid interface, where interface mass transfer occurs.

6. Acknowledgement

Naveen Weerasekera and Aurelie Lagurre wish to thank Dr. Elliott Gall (Department of Mechanical and Materials Engineering- Portland State University) for his constant support for succession of this wok.

7. Funding

This work was performed by the funding provided by the Department of Mechanical and Materials Engineering of Portland State University and Portland State Institute for Sustainable Solutions STARR Research Grant.

References

[1] M.K. Jain, "Introduction to Biological Membranes (Second Edition)", "*FEBS LETTERS*", Vol. 238 (1), 1988
[2] R. Soria, "Overview on industrial membranes", "*Catalysis Today*", Vol. 25 (3-4), 1995, 285-290
[3] P.M. Bungay, H.K. Lonsdale, M.N. DePinho, "Synthetic membranes: Science, engineering and applications", "*D Reidel Publishing*", 1983
[4] Ryan Huizing, Walter Merida, Frank Ko, "Impregnated electrospun nanofibrous for water vapor transport applications", "*Journal of Membrane Science*", Vol. 461. 146-160
[5] A. Mardiana Idau, S.B Riffat, "Review on heat recovery technologies for building applications", "*Renewable and Sustainable Energy Reviews*", Vol. 16 (2), 2012, 1241-1255
[6] Mohammadreza Omidkhah, Mona Zamani Pedram and Abtin Ebadi Amooghin, "Facilitated Transport of CO2 through EA-Mediated Poly(Vinyl alcohol)Membrane Cross-Linked by Formaldehyde", *Journal of Membrane Science and Technology*", DOI: 10.4172/2155-9589.1000119, LONGDOM Publishing
[7] Benamar Dahmani, Mustapha Chabane, "Study of Membrane Fouling and Trihalomethane Formation in Reverse Osmosis Desalination Pilot Unit", "*Journal of Membrane Science and Technology*", Vol. 1 (4), 2011
[8] Mustafa J, Farhan M, Hussain M, "CO_2 Separation from Flue Gases Using Different Types of Membranes", "*Journal of Membrane Science and Technology*", Vol. 6 (2), 2016, Longdom Publishing
[9] Tjoon Tow Teng, Muthuraman G, Mubeena K, Sathya M, "Emulsion Liquid Membrane: Removal and Recovery of Organic and Inorganic Ions", "*Journal of Membrane Science and Technology*", Vol. 3 (2), 2013, Longdom Publishing
[10] Lalit M. Pant, Susantha K. Mishra, Marc Secanell, "Absolute permeability and Knudsen diffusivity measurements in PRMFC gas diffusion layer and microporous layers", "*Journal of Power Sources*", Vol. 206 (2012), 153-160
[11] J. Phattaranawik, R. Jiraratananon, A.G. Fane, "Effect of pore size distribution and air flux on mass transport in direct contact membrane distillation", "*Journal of Membrane Science*", 215 (2003), 75-85
[12] Min-Gyun Park, Tuncer B. Edil, Craig H. Benson, "Modeling Volatile Organic Compound Transport in Composite Liners", "*Journal of Geotechnical and Geo-environmental Engineering*", 2012, 138(6): 641-657
[13] L.Z. Zhang, Y. Jiang, "Heat and mass transfer in a membrane-based energy recovery ventilator", "*Journal of Membrane Science*", 163 (1999) 29-38
[14] Ryan Huizing, Hao Chen, Frankie Wong, "Contaminant transport in membrane-based energy recovery ventilators", "*Science and Technology for The Built Environment*" (2015) 21, 54–66
[15] Jinzhe Nie, Jianrong Yang, Lei Fang, Xiangrui Kong, "Experimental evaluation of enthalpy efficiency and gas-phase contaminant transfer in an enthalpy recovery unit with polymer membrane foils", "*Science and Technology for the Built Environment*" (2015) 21, 150–159
[16] Doyun Wona, Daniel M. Sandera, C.Y. Shawa, Richard L. Corsi, "Validation of the surface sink model for sorptive interactions between VOCs and indoor materials", "*Atmospheric Environment*" 35 (2001) 4479–4488
[17] Yufeng He, Nigel A. Seaton, "Monte Carlo Simulation and Pore-Size Distribution Analysis of the Isosteric Heat of Adsorption of Methane in Activated Carbon", "*Langmuir"* 2005, 21, 18, 8297-8301
[18] Mehdi Dehghan, "Numerical solution of the three-dimensional advection-diffusion equation", "*Applied Mathematics and Computation*", 150 (2004) 5-19

Author Profile

Naveen Daham Weerasekera is a former graduate research assistant at the Department of Mechanical and Materials Engineering of Portland State University, Portland OR, USA, He obtained his master's degree in mechanical engineering from Portland State University and bachelor's degree from National Institute of Technology-Silchar, INDIA. He is an active researcher in microfluidics and particle dynamics. His research is funded by STARR research grant awarded by the Portland State Institute for Sustainable Solutions (ISS), USA

Aurelie Laguerre is a research analyst in analytical chemistry and a research scientist at the Department of Mechanical and Materials Engineering of Portland State University, Portland OR, USA. She is specialized in Proton Transfer Reaction Mass Spectrometry (PTR-MS), Gas Chromatographic Mass Spectrometry (GCMS) and environmental chemistry. Her research interest is on atmospheric pollutant dynamics.